Supplementary Information

Microstructure engineering of polyamide membranes for ultrafast polar and non-polar solvent transport

Huiqing Wu[1,2,*], Yang Xu[1], Qingchen Tang[3], Baohu Wu[4], Peiyi Wu[1,*]

[1]State Key Laboratory of Advanced Fiber Materials (Donghua University), College of Chemistry and Chemical Engineering, Donghua University, Shanghai 201620, China

[2]National Innovation Center of Advanced Dyeing and Finishing Technology, Tai'an, Shandong 271000, China

[3]State Key Laboratory of Advanced Fiber Materials (Donghua University), Center for Advanced Low-Dimension Materials, and College of Materials Sciences and Engineering, Donghua University, Shanghai 201620, China

[4]Jülich Centre for Neutron Science (JCNS) at Heinz Maier-Leibnitz Zentrum (MLZ) Forschungszentrum Jülich, Lichtenbergstr. 1, 85748 Garching, Germany

Correspondence should be addressed to H.Q.W. (email: huiqingwu@dhu.edu.cn) and P.Y.W. (email: wupeiyi@dhu.edu.cn)

This file includes

Supplementary Notes 1-7

Supplementary Fig.1. Distribution of electrostatic potential and corresponding extreme points at the molecular van der Waals surface

Supplementary Fig.2. MSD curves, FTIR spectra of DES and ODA-dissolved DES solution. Interactions between DES and ODA by DFT calculation

Supplementary Fig.3. FTIR spectrum of ODA monomer and ODA/TMC membrane

Supplementary Fig.4. Pore size distribution for ODA/TMC and MPD/TMC samples obtained from CO_2 isotherms at 273 K

Supplementary Fig.5. ζ-potential of the surface of ODA/TMC TFC membrane at pH=3 ~ 11

Supplementary Fig.6. TGA curve for the ODA/TMC TFC membrane under nitrogen atmosphere

Supplementary Fig.7. SEM images of the surfaces of the ODA/TMC TFC membranes prepared with different reaction time

Supplementary Fig.8. XPS survey and narrow scan spectra of ODA/TMC TFC membrane
Supplementary Fig.9. Effect of ODA and NaOH concentration on the methanol permeance and RB19 rejection of ODA/TMC TFC membrane
Supplementary Fig.10. Rejection of dyes with different molecular weights in methanol
Supplementary Fig.11. Solution photographs of feed and permeate containing different dyes in methanol after filtration. The optical images of membrane surfaces before and after filtration experiments shown at each of the bottom
Supplementary Fig.12. Analysis of solvent transport through ODA/TMC TFC membrane
Supplementary Fig.13. Permeance of ODA/TMC TFC membrane under different pressures
Supplementary Fig.14. Stability of ODA/TMC TFC membrane towards various solvents
Supplementary Fig.15. Calculation of entrance resistances and passage resistances to solvent permeation across the ODA/TMC membrane
Supplementary Fig.16. Mean square displacement of methanol and hexane molecules as a function of time in the ODA/TMC membrane

Supplementary Table 1. Distribution coefficients of monomers between different solvents
Supplementary Table 2. Interfacial tension between cyclohexane and different solvents
Supplementary Table 3. Properties of the representative dyes used in this work
Supplementary Table 4. Values of the group contributions for estimation of the solubility parameter of the polyamide from Hoy's system
Supplementary Table 5. Solubility parameters of solvents and polyamide
Supplementary Table 6. Solubility parameter differences between solvents and polyamide
Supplementary Table 7. Calculation of Flory-Huggins interaction parameters for ODA/TMC polyamide
Supplementary Table 8. Properties of solvents used for nanofiltration test
Supplementary Table 9. Comparison between the ODA/TMC TFC membrane and previously reported membranes
Supplementary Table 10. Non-bonded parameters and general amber force field (GAFF2) used

Supplementary References 1-22

Supplementary Notes

Supplementary Note 1. Molecular dynamic simulation for the amine monomer diffusion

Molecular dynamic simulation was operated to calculate the diffusion rate of amine monomer in DES and water system. The diffusion coefficients of amine monomer molecules could be estimated from the slope of mean square displacement (MSD) curves in Supplementary Fig. 2a-c by the Einstein relationship. The higher slope of the MSD curve, the fast diffusion rate. In comparison with in water, the diffusion rates of amine monomer in DES could be obviously retarded, especially for ODA with a large molecule size. From FTIR spectrum (Supplementary Fig. 2d), the observed shift to low wavenumber suggest the hydrogen bonding interactions between ODA and DES. However, the shift is slight, probably as a result of low concentration of ODA (1%) in the DES. Furthermore, density-functional theory (DFT) calculations was also performed (Supplementary Fig. 2e). There are strong hydrogen bonding interactions (blue and green regions) between ODA and DES, including N-H···Cl^- and OH···N-H, suggesting ODA can partake in the hydrogen bonding network of DES phase as a hydrogen-bond donor. Therefore, the diffusion rate of ODA monomers is slow down, through the synergetic effect of high viscosity of DES and the strong hydrogen bonding interactions between ODA and DES.

Supplementary Note 2. Calculation for the partition coefficients

To investigate the monomer diffusion mechanism across the alkane/DES interface, as shown in Supplementary Table 1, the partition coefficient ($logP_{A/B}$) of monomers (ODA or TMC) between immiscible solvents A (cyclohexane) and B (water or DES) was calculated.

The $logP_{cyclohexane/DES}$ and $logP_{cyclohexane/water}$ of TMC are -0.51 and 2.64, respectively, indicating that TMC is easier to diffuse into DES rather than into water from cyclohexane. The $logP_{cyclohexane/water}$ and $logP_{cyclohexane/DES}$ of MPD are -2.47 and -3.52, respectively, suggesting that MPD is more difficult to diffuse into cyclohexane from DES than water. Similarly, the $logP_{cyclohexane/water}$ (-1.17) and $logP_{cyclohexane/DES}$ (-3.53) of ODA also suggest that ODA is more difficult to diffuse into cyclohexane from DES than water.

Thus, the diffusion of TMC in DES/hexane is predominant, and the polymerization occurs at DES side when TMC diffuses from the cyclohexane phase into DES phase and reacts with amine monomers. Thus, through the modulation of thermodynamic partitioning and kinetic, there is an opposite diffusion of monomers and reaction position at alkane/DES interface, compared to the conventional IP at the alkane/water interface.

Supplementary Note 3. Calculation for the solubility parameters

The Equation S1-S7 are used for estimation of the solubility parameter (δ_0) in Hoy's system in Supplementary Table 5. Here, B=base value=277.

$$\alpha^{(p)} = 777\Delta T^{(p)}/V \quad (S1)$$

$$n = 0.5/\Delta T^{(p)} \quad (S2)$$

$$\delta_t = (F_i + B/n)/V \quad (S3)$$

$$\delta_p = \delta_t\left(\frac{1}{\alpha}\frac{F_p}{F_t+B/n}\right)^{1/2} \quad (S4)$$

$$\delta_h = \delta_t[(\alpha^{(p)} - 1/\alpha^{(p)}]^{1/2} \quad (S5)$$

$$\delta_d = (\delta_t{}^2 - \delta_p{}^2 - \delta_h{}^2)^{1/2} \quad (S6)$$

$$\delta_0 = (\delta_d{}^2 + \delta_p{}^2 + \delta_h{}^2)^{1/2} \quad (S7)$$

Supplementary Note 4. Calculation for the solubility parameter difference

The solubility parameter difference ($\Delta\delta_{s\text{-}p}$) between a solvent and polymer, where "s" and "p" represents the solvent and the polyamide made from ODA/TMC or MPD/TMC, respectively. The solubility parameter difference is calculated corresponding to the following Equation S8:

$$\Delta\delta_{s\text{-}p} = [(\delta_{d,p} - \delta_{d,s})^2 + (\delta_{p,p} - \delta_{p,s})^2 + (\delta_{h,p} - \delta_{h,s})^2]^{1/2} \quad (S8)$$

To investigate the interactions between the polyamide and solvent molecules, the solubility parameter differences ($\Delta\delta_{s\text{-}p}$) were calculated. Four representative organic solvents including polar solvents (methanol, acetone) and non-polar solvents (hexane, toluene) were chosen. ODA/TMC and MPD/TMC polyamide were studied and compared to understand the influence of composition. The fully cross-linked and linear polyamide networks from ODA/TMC and MPD/TMC were all discussed, taking account of the different cross-linking degrees.

Generally speaking, the smaller value of the $\Delta\delta_{s\text{-}p}$, the stronger interaction exists between the solvent and the polymer. As shown in Table S6, regarding both fully cross-linked and linear MPD/TMC polyamide, $\Delta\delta_{s\text{-}p}$ for polar solvents is small (<11 $MPa^{1/2}$) and for non-polar solvents is high (~20 $MPa^{1/2}$), giving a brief account of high polar solvents' permeance but ultralow non-polar solvents' permeance for conventional MPD/TMC membranes. Compared with MPD/TMC polyamide, both fully cross-linked and linear ODA/TMC polyamide exhibits a similar or smaller $\Delta\delta_{s\text{-}p}$ for polar solvents (<10 $MPa^{1/2}$), suggesting good interactions towards polar solvents. Moreover, it is also found all the values of $\Delta\delta_{s\text{-}p}$ for non-polar solvents are also dramatically decreased. It is revealed that ODA/TMC polyamide could interact moderately with non-polar solvents, which could be ascribed to the extra benzene rings in the polyamide network brought by ODA. Thus, the enhanced alternating distribution of hydrophilic and hydrophobic

domains endow the ODA/TMC membrane with a Janus structure that hold desirable affinity with both polar and non-polar solvents.

Supplementary Note 5. Calculation of Flory-Huggins interaction parameters

To further measure the possible interactions between polyamide and solvents as well as the swelling of the membranes, the polymer-solvent interaction parameter chi (χ) described by Flory–Huggins interaction parameter equation as shown below Equation S9 is used.

$$\chi = \beta + (\frac{V_s}{RT})(\delta_s - \delta_p)^2 \quad \text{(S9)}$$

where β is lattice constant of value ~0.34.

Classically, when the value of $\chi > 2.0$, there are small interactions between polymer and solvent, while the good interactions are predicted with $0.5 < \chi < 2.0$. When $\chi < 0.5$, the interactions are so strong that solvation or swelling may occur.

Supplementary Note 6. Calculation for the entrance and passage resistances

Based on Hagen-Poiseuille's equation, the resistance to flow in the pore could be expressed as Equation S10:

$$\frac{\Delta P}{Q} = \frac{8\eta t}{\pi R^4} \quad \text{(S10)}$$

For an infinitely thin membrane, the resistance to the flow across the pore could be described by Sampson's equation as Equation S11:

$$\frac{\Delta P}{Q} = \frac{3\eta}{R^3} \quad \text{(S11)}$$

Thus, the whole resistance through ODA/TMC NF membrane could be obtained from the superimposition by Equation S10 and 11:

$$\frac{\Delta P}{Q} = \frac{3\eta}{R^3} + \frac{8\eta t}{\pi R^4} \quad \text{(S12)}$$

The relative contributions of entrance and passage could be quantified by assessing the thickness-to-pore radius aspect ratio (L/R). When the entrance resistance equals to pore resistance, the critical value of L/R is 1.18. For ODA/TMC NF membrane with a thickness (L) of ~12 nm, pore radius (R) of ~0.40 nm, L/R is calculated to be ~30.

The higher thickness-to-pore radius aspect ratio reveals the domination of pore passage resistance in mass transport, where the resistance for pore passage is approximately 26 times higher than entrance resistance (Supplementary Fig. 15). Thus, a viscous flow passage-dominated permeation mechanism is proposed for the membrane.

Supplementary Note 7. MD calculation using non-bonded parameters and general amber force field

MD simulation parameters:

The interaction potentials V between atoms include the bonded and non-bonded terms.

$$V=V_{bonded}+V_{non\text{-}bonded} \quad \text{(S13)}$$

The bonded terms include the harmonic oscillation of bonds and angles as well as the torsional rotation of dihedrals; the non-bonded term include the electrostatic interactions between atoms with partial charges as well as the Van der Waals interactions described through the Lennard-Jones potentials.

$$V_{bonded}=\sum_{bonds}\frac{1}{2}k_b(l-l_0)^2+\sum_{angles}\frac{1}{2}k_\theta(\theta-\theta_0)^2+\sum_{torsions}k_\phi\left[1+\cos\left(n\phi-\phi_0\right)\right] \quad \text{(S14)}$$

$$V_{non\text{-}bonded}=\sum_{i=1}^{N}\sum_{j=i+1}^{N}\left\{\frac{q_iq_j}{4\pi\epsilon_0\epsilon_r r_{ij}}+4\varepsilon_{ij}\left[\left(\frac{\sigma_{ij}}{r_{ij}}\right)^{12}-\left(\frac{\sigma_{ij}}{r_{ij}}\right)^{6}\right]\right\} \quad \text{(S15)}$$

Supplementary Figures

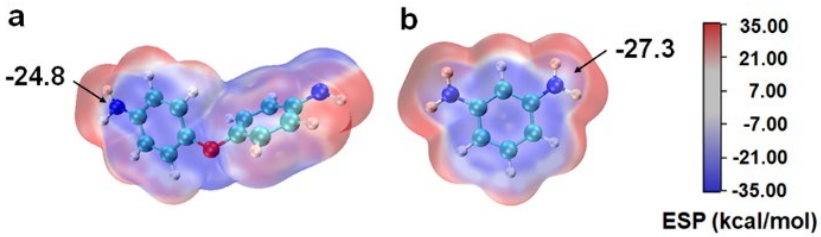

Supplementary Fig. 1. Distribution of electrostatic potential and corresponding extreme points at the molecular van der Waals surface: a) ODA, b) MPD.

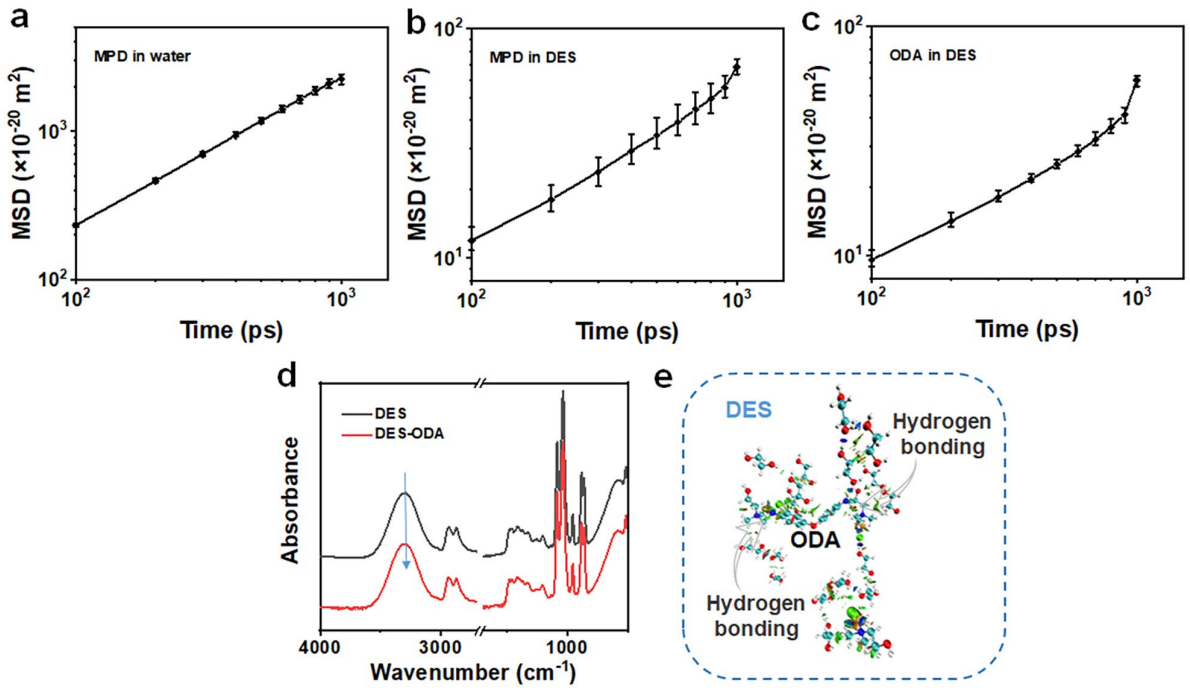

Supplementary Fig. 2. MSD curves: a) MPD in water, b) MPD in DES, c) ODA in DES. **e) FTIR spectra of DES and ODA-dissolved DES solution. f) Interactions between DES and ODA by DFT calculation.**

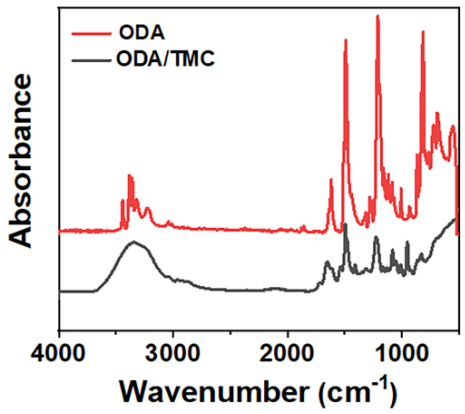

Supplementary Fig. 3. FTIR spectrum of ODA monomer and ODA/TMC membrane.

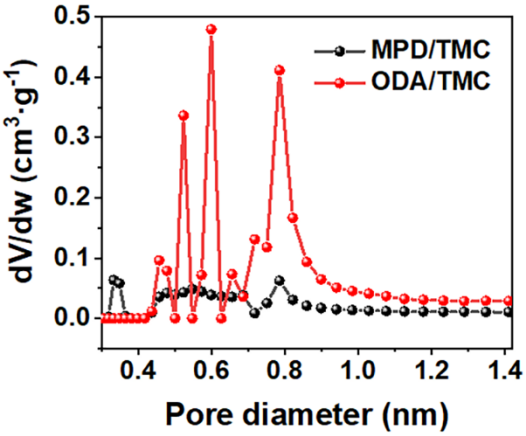

Supplementary Fig. 4. Pore size distribution for ODA/TMC and MPD/TMC samples obtained from CO_2 isotherms at 273 K.

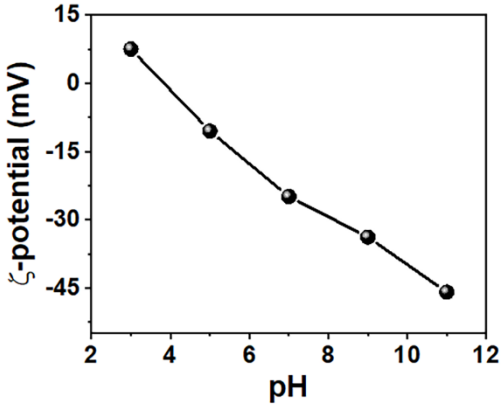

Supplementary Fig. 5. ζ -potential of the surface of ODA/TMC TFC membrane at pH=3 ~ 11.

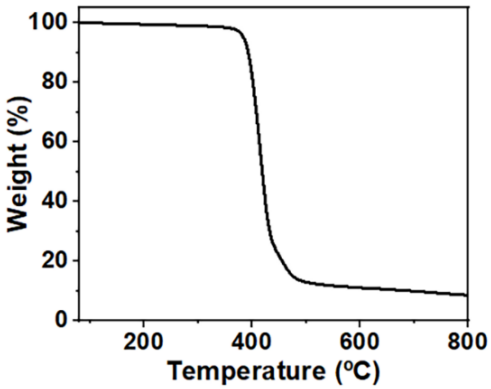

Supplementary Fig. 6. TGA curve for the ODA/TMC TFC membrane under nitrogen atmosphere.

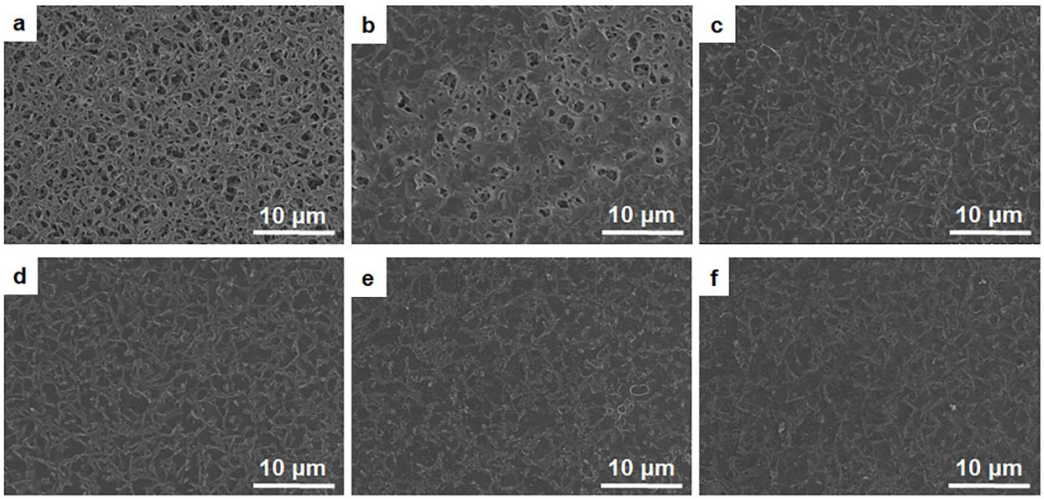

Supplementary Fig. 7. SEM images of the surfaces of the ODA/TMC TFC membranes prepared with different reaction time: a) Nylon substrate, b) 45 s, c) 60 s, d) 75 s, e) 90 s, f) 120 s.

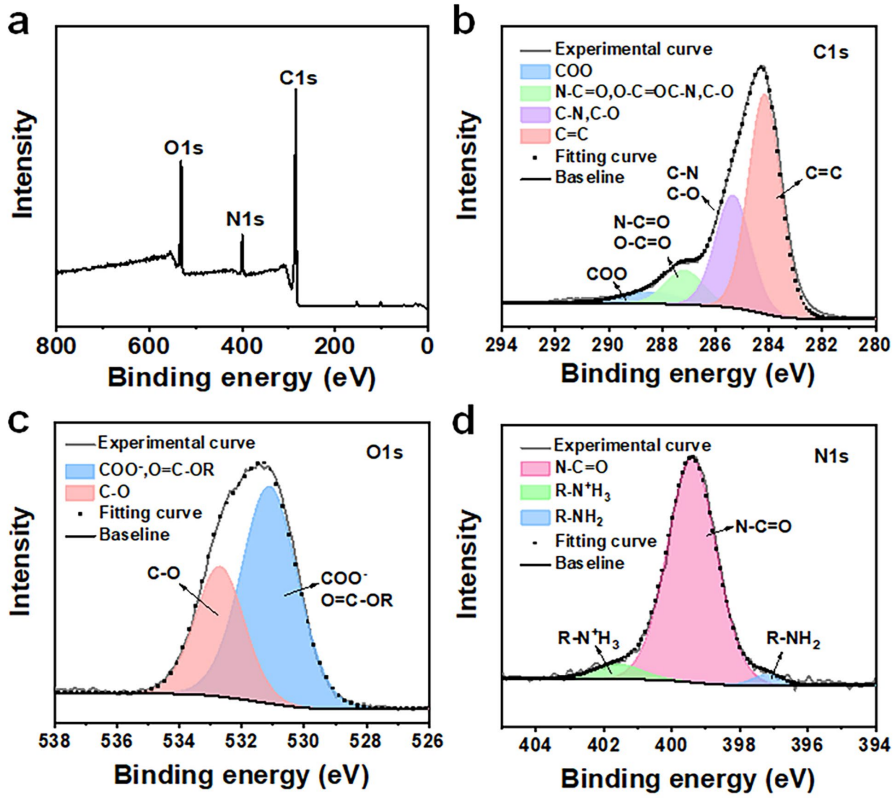

Supplementary Fig. 8. XPS survey and narrow scan spectra of ODA/TMC TFC membrane: a) Whole survey. Narrow scan spectra of b) C1s, c) O1s and d) N1s.

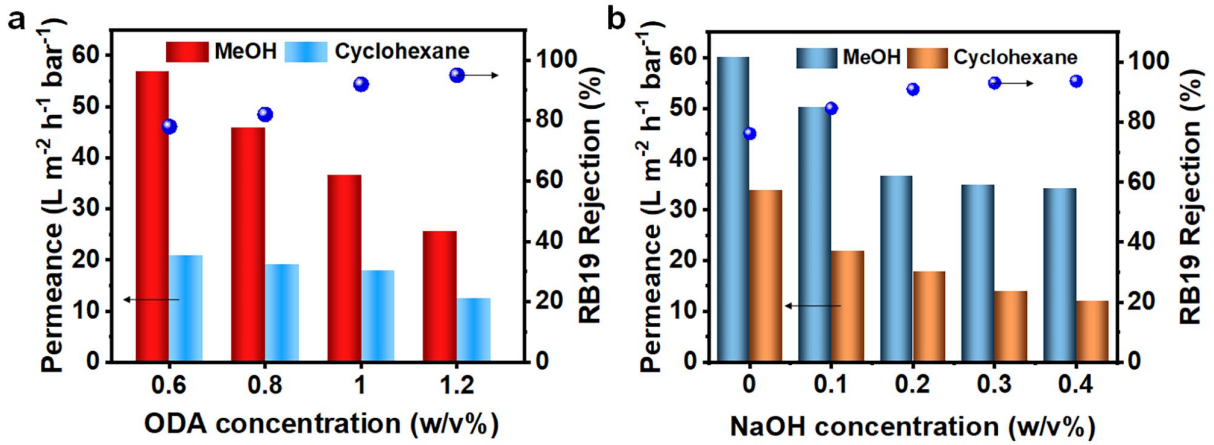

Supplementary Fig. 9. Effect of a) ODA and b) NaOH concentration on the membrane performance.

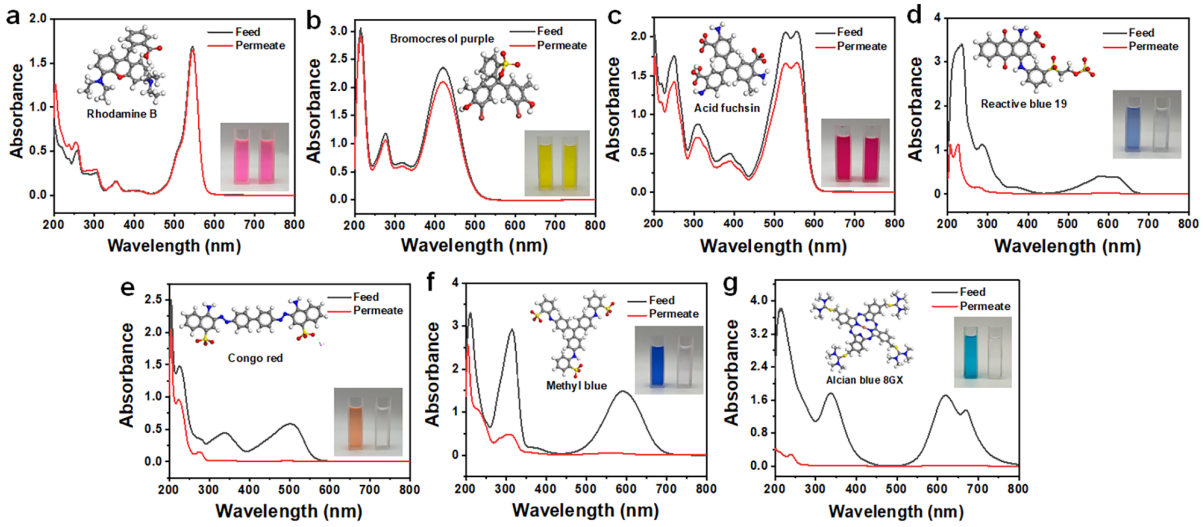

Supplementary Fig. 10. Rejection of dyes with different molecular weights in methanol: a) Rhodamine B, b) Bromocresol purple, c) Acid fuchsin, d) Reactive blue 19, e) Congo red, f) Methyl blue, g) Alcian blue 8GX.

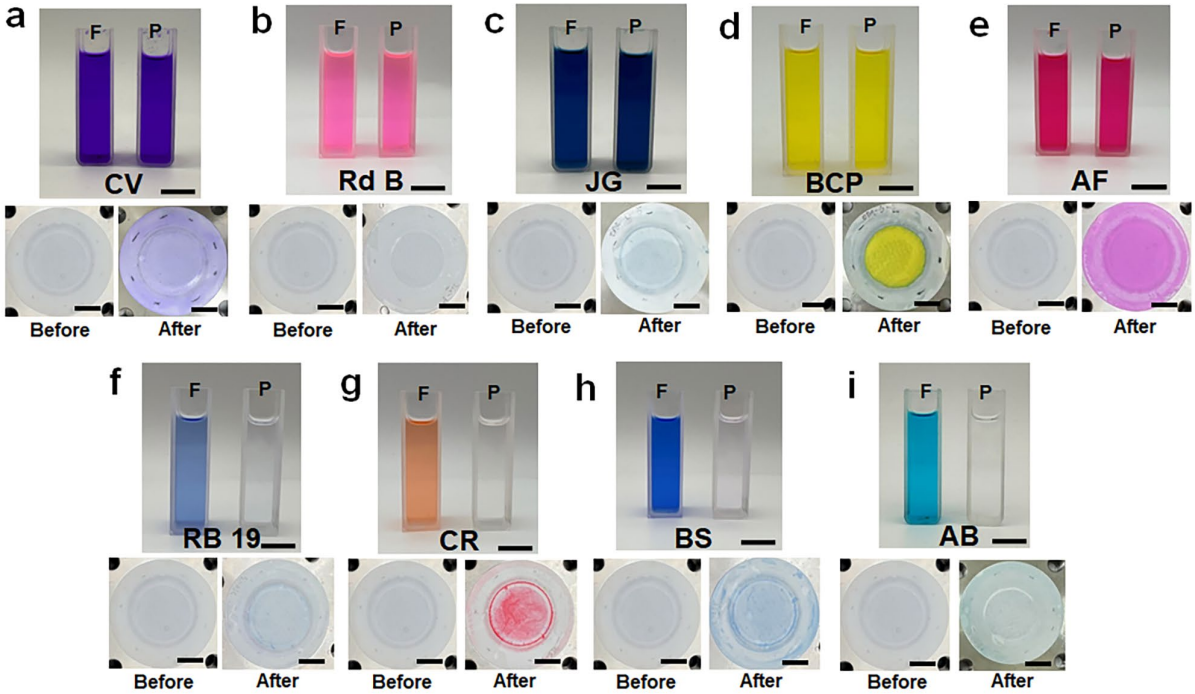

Supplementary Fig. 11. Solution photographs of feed (F) and permeate (P) containing different dyes in methanol after filtration. The optical images of membrane surfaces before and after filtration experiments shown at each of the bottom. Scale bar: 1 cm. (a) Rd B, (b) CV, (c) JG, (d) BCP, (e) AF, (f) RB 19, (g) CR, (h) BS, (i) AB.

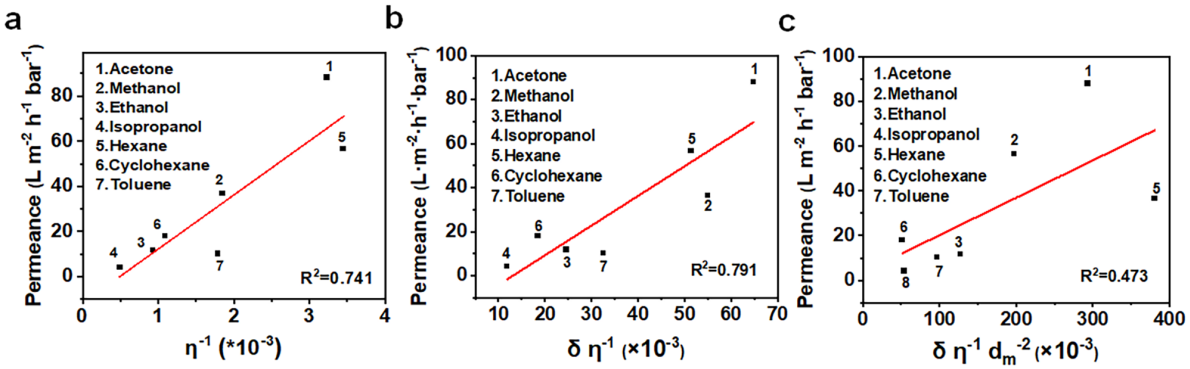

Supplementary Fig. 12. Analysis of solvent transport through ODA/TMC TFC membrane. Plot and fitting of solvent permeance against the combined solvent property: a) Viscosity, b) Total solubility parameter and viscosity, c) Total solubility parameter, molar diameter and viscosity.

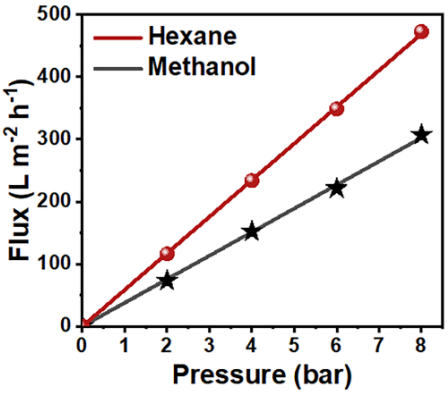

Supplementary Fig. 13. Permeance of ODA/TMC TFC membrane under different pressures.

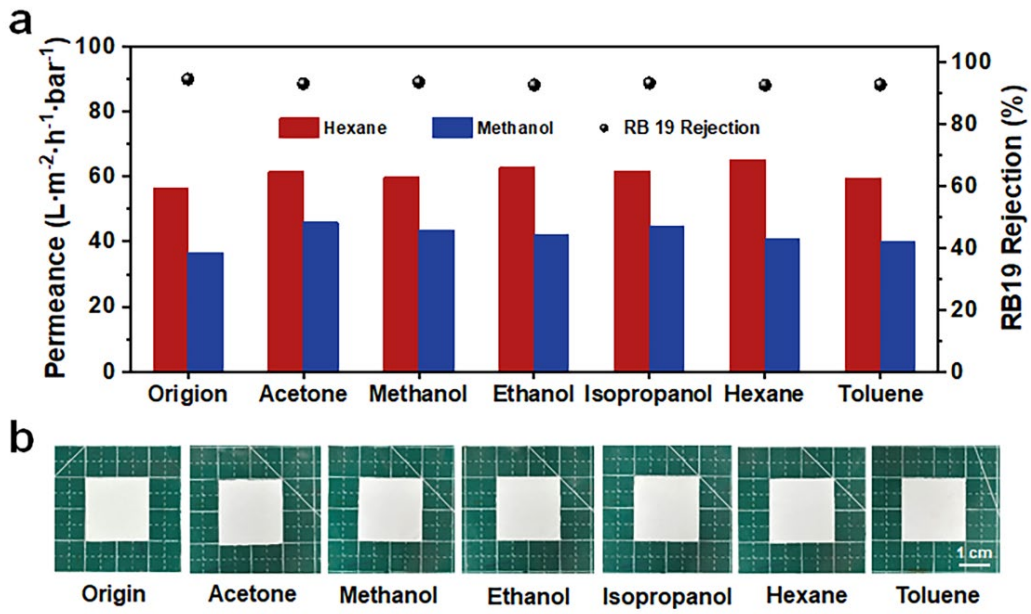

Supplementary Fig. 14. Stability of ODA/TMC TFC membrane towards various solvents. a) Solvent permeance and RB19 rejection, b) Photo images of origin ODA/TMC TFC membrane and after the immersion in various solvents for 4 days.

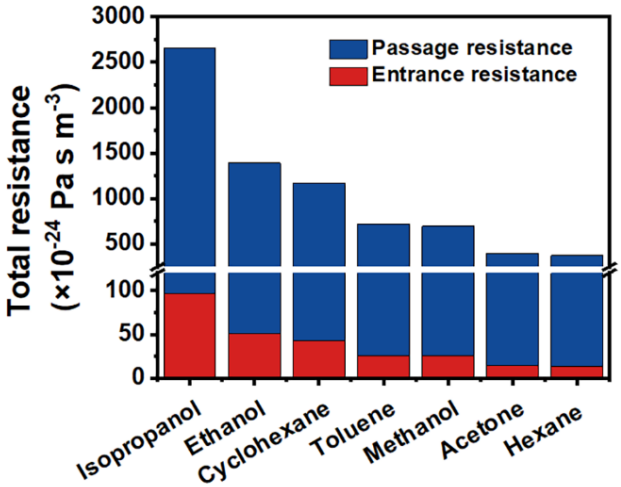

Supplementary Fig. 15. Calculation of entrance resistances and passage resistances to solvent permeation across the ODA/TMC membrane.

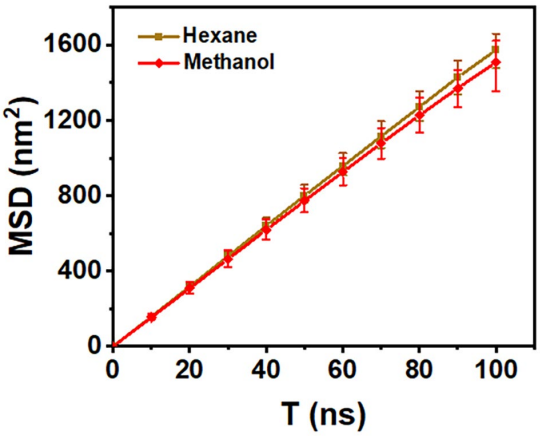

Supplementary Fig. 16. Mean square displacement of methanol and hexane molecules as a function of time in the ODA/TMC membrane.

Supplementary Tables

Supplementary Table 1. Distribution coefficients of monomers between different solvents.

Monomer	Solvent	E (Hartree)	Log $P_{A/B}$ (J mol^{-1})
ODA	cyclohexane	-649.044735	/
	water	-649.047291	-1.17
	DES	-649.052420	-3.53
MPD	cyclohexane	-342.857112	/
	water	-342.862474	-2.47
	DES	-342.864764	-3.52
TMC	cyclohexane	-1951.003390	/
	water	-1950.997652	2.64
	DES	-1951.002288	-0.51

Supplementary Table 2. Interfacial tension (mN m^{-1}) between cyclohexane and different solvents.

	Cyclohexane	Water	DES
Air	24.1	70.9	51.0
Cyclohexane	-	45.5	18.3

Supplementary Table 3. Properties of the representative dyes used in this work.

Name	M_W (g mol^{-1})	Structure	Dimension (Å)	Charge
Crystal violet (CV)	408	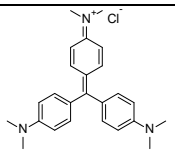	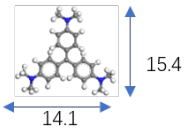	+1
Rhodamine B (Rd B)	479	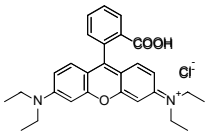	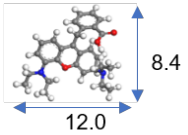	+1
Janus green (JG)	511.1	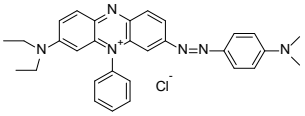	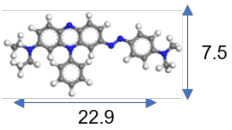	+1
Bromocresol purple (BCP)	540.2	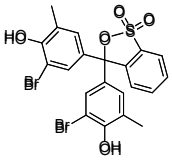	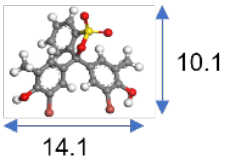	0
Acid fuchsin (AF)	585.5	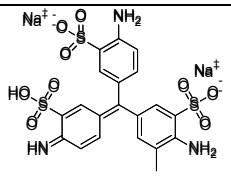	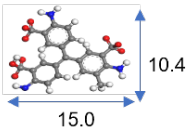	-2
Reactive blue 19 (RB 19)	626.5	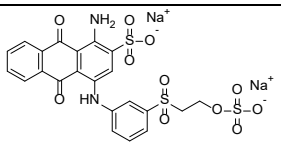	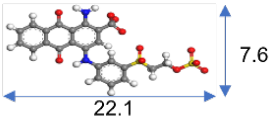	-2
Congo red (CR)	696.7	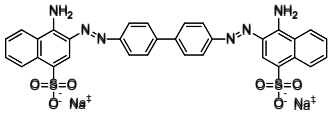	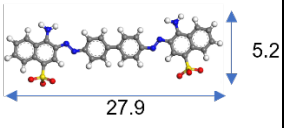	-2
Methyl blue (BS)	799.8	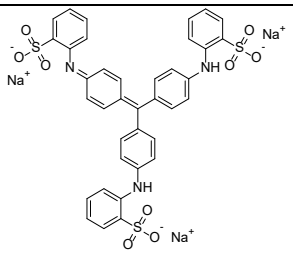	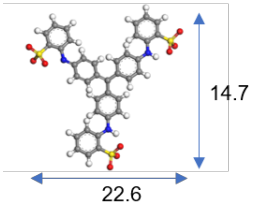	-3
Alcian blue 8GX (AB)	1298.9	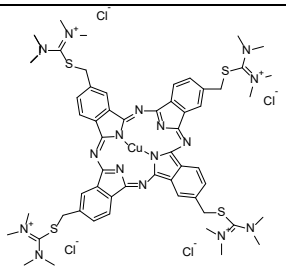	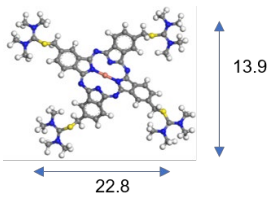	+3

Supplementary Table 4. Values of the group contributions for estimation of the solubility parameter of the polyamide from Hoy's system (1985) [1].

Groups	Numbers				$F_{t,i}$	$F_{p,i}$	V_i	$\Delta T_{T,I}^{(P)}$
					$((MJ/m^3)^{1/2}/mol)$		(cm^3/mol)	
CH(aromatic)	11	15	7	9	241	62.5	13.42	0.018
C(aromatic)	7	9	5	6	201	65	7.42	0.015
-CONH-	2	3	2	3	1131	895	28.3	0.073
-COOH	1	0	1	0	241	62.5	13.42	0.018
-O-(ether)	1	1.5	0	0	235	216	6.45	0.018
Sum	A*				6798	3211	276.03	0.485
		B*			9169.5	4531.5	362.655	0.651
			C*		5519	2967.5	213.74	0.386
				D*	6768	3637.5	250.2	0.471

*A, B, C, D presents the linear ODA/TMC, fully cross-linked ODA/TMC, linear MPD/TMC, fully cross-linked MPD/TMC, respectively.

Supplementary Table 5. Solubility parameters of solvents and polyamide[1, 2].

Solubility parameters	δ_d ($MPa^{1/2}$)	δ_p ($MPa^{1/2}$)	δ_h ($MPa^{1/2}$)	δ_0 ($MPa^{1/2}$)
Methanol	15.1	12.3	22.3	29.7
Acetone	15.5	10.4	7.0	20.1
Hexane	14.9	0	0	14.9
Toluene	18.0	1.4	2.0	18.2
Linear ODA/TMC	16.2	14.8	13.2	25.6
Fully cross-linked ODA/TMC	16.3	15.3	13.9	26.3
Linear MPD/TMC	15.7	16.3	14.4	26.8
Fully cross-linked MPD/TMC	16.1	16.7	15.8	28.1

Supplementary Table 6. Solubility parameter differences ($\Delta\delta_{s-p}$) between solvents and polyamide.

Solvent	Linear polyamide		Fully cross-linked polyamide	
	$\Delta\delta_{s-p}$ (ODA/TMC) ($MPa^{1/2}$)	$\Delta\delta_{s-p}$ (MPD/TMC) ($MPa^{1/2}$)	$\Delta\delta_{s-p}$ (ODA /TMC) ($MPa^{1/2}$)	$\Delta\delta_{s-p}$ (MPD/TMC) ($MPa^{1/2}$)
Methanol	9.5	8.9	9.0	7.9
Acetone	7.63	9.5	8.5	10.8
Hexane	19.9	21.8	20.7	23
Toluene	17.6	19.5	18.4	20.7

Supplementary Table 7. Calculation of Flory-Huggins interaction parameters for ODA/TMC polyamide[2, 3, 4].

	PA-methanol		PA-acetone		PA-hexane		PA-toluene	
	Linear	Fully cross-linked	Linear	Fully cross-linked	Linear	Fully cross-linked	Linear	Fully cross-linked
β	0.34							
V_s (cm^3/mol)	40.7		73.9		131.6		106.8	
R (cm^3/Pa K/mol)	8314000							
T (K)	298.15							
χ	0.616	0.530	1.67	1.48	6.42	7.42	2.7	3.17

Supplementary Table 8. Properties of solvents used for nanofiltration test.

Solvent	Molar volume (V_m)(cm^3 mol^{-1})	Diameter (d_m)(nm)	Viscosity (10^{-3} Pa·s)	Hansen solubility parameter ($MPa^{1/2}$)			
				δ_d	δ_p	δ_h	δ_0
Acetone	73.9	0.47	0.31	15.5	10.4	7.0	20.1
Methanol	40.7	0.38	0.54	15.1	12.3	22.3	29.7
Ethanol	58.5	0.44	1.08	15.8	8.8	19.4	26.6
Isopropanol	76.8	0.47	2.06	15.8	6.1	16.4	24.6
Hexane	131.6	0.51	0.29	14.9	0	0	14.9
Toluene	106.8	0.58	0.56	18.0	1.4	2.0	18.2
Cyclohexane	107.9	0.60	0.91	16.8	0	0.2	16.8

Supplementary Table 9. Comparison between the ODA/TMC TFC membrane and previously reported membranes.

Membrane	Permeance (L h^{-1} m^{-2} bar^{-1})		MWCO (Da)	Reference
	Methanol	Hexane		
BIPOL/TMC	17.2	0.4	314	[4]
Amino–CD/TPC	17.5	16	475	[5]
MPCM/TPC	38.5	65	450	[6]
BAF/TMC	23.88	4	585	[7]
p-CMP/TEB	22	32	590	[8]
TAPB/TFPA	16	4.7	687	[9]
β-CD/TMC	4.9	6.3	400	[10]
TpBD	8.3	0	305	[11]
PANI	23	5.4	500	[12]
MPD/TMC	7	0.2	327	[13]
m-XDA/TMC	12.5	1.5	300	[14]
N4/TPC	6.2	0	680	[15]
MOA/TMC	20	62	450	[16]
β-CDA/TPC	6	0.23	351	[17]
Tren-TFE/TMC	20.7	15	500	[18]
PEI (Co^{2+})/TMC	18	2.5	450	[19]
6FAP/TMC	13	0.7	388	[20]
33DT	24.2	~59	540	[21]
This work	36.9	56.6	625	

Supplementary Table 10. Non-bonded parameters and general amber force field (GAFF2) used.

$V_{non\text{-}bonded}$	q(e)	ε_{ij} (KJ/mol)	σ_{ij} (nm)
c3s	0.48	0.27614	0.35003
f	-0.23	0.27614	0.29809
o	-0.73	0.87864	0.29596
s6	1.40	1.04600	0.35458
c3	0.109900	4.57730e-01	3.39967e-01
h1	0.049450	6.56888e-02	2.47135e-01
oh	-0.597800	8.80314e-01	3.06647e-01
ho	0.401500	0.00000e+00	0.00000e+00
os	-0.417600	7.11280e-01	3.00001e-01
hc	0.044367	6.56888e-02	2.64953e-01
h1	0.018700	6.56888e-02	2.47135e-01

Supplementary references

1. Van Krevelen DW, Te Nijenhuis K. Properties of polymers: Their correlation with chemical structure; their numerical estimation and prediction from additive group contributions. *Elsevier* (2009).
2. Hansen CM. Hansen solubility parameters: A user's handbook. *CRC press* (2007).
3. Ghazali NF, Md Hanim K, Pahlawi QA, Lim KM. Enrichment of carotene from palm oil by organic solvent nanofiltration. *J. Am. Oil Chem. Soc.* **99**, 189-202 (2022).
4. Bhanushali D, Kloos S, Kurth C, Bhattacharyya D. Performance of solvent-resistant membranes for non-aqueous systems: solvent permeation results and modeling. *J. Membr. Sci.* **189**, 1-21 (2001).
5. Li S-L, et al. 2,2'-Biphenol-based ultrathin microporous nanofilms for highly efficient molecular sieving separation. *Angew. Chem. Int. Ed.* **61**, e202212816 (2022).
6. Huang T, Puspasari T, Nunes SP, Peinemann K-V. Ultrathin 2D-layered cyclodextrin membranes for high-performance organic solvent nanofiltration. *Adv. Funct. Mater.* **30**, 1906797 (2020).
7. Huang T, et al. Molecularly-porous ultrathin membranes for highly selective organic solvent nanofiltration. *Nat. Commun.* **11**, 5882 (2020).
8. Sun Y, et al. Rigid twisted structured PA membranes for organic solvent nanofiltration via co-solvent assisted interfacial polymerization. *J. Membr. Sci.* **666**, 121179 (2023).
9. Liang B, et al. Microporous membranes comprising conjugated polymers with rigid backbones enable ultrafast organic-solvent nanofiltration. *Nat. Chem.* **10**, 961-967 (2018).
10. Alduraiei F, Kumar S, Liu J, Nunes SP, Szekely G. Rapid fabrication of fluorinated covalent organic polymer membranes for organic solvent nanofiltration. *J. Membr. Sci.* **648**, 120345 (2022).
11. Liu J, Hua D, Zhang Y, Japip S, Chung T-S. Precise molecular sieving architectures with Janus pathways for both polar and nonpolar molecules. *Adv. Mater.* **30**, 1705933 (2018).
12. Guo H, et al. Tailor-made β-ketoenamine-linked covalent organic polymer nanofilms for precise molecular sieving. *Mater. Horiz.* **10**, 5133-5142 (2023).
13. He P, et al. In-situ growth of double-layered polyaniline composite membrane for organic solvent nanofiltration. *Chem. Eng. J.* **420**, 129338 (2021).
14. Fu W, et al. Polyamide composite membrane with 3D honeycomb-like structure via acetone-regulated interfacial polymerization for high-efficiency organic solvent

nanofiltration. *J. Membr. Sci.* **679**, 121711 (2023).

15. Hu YX, et al. Two copolymer-grafted silica stationary phases prepared by surface thiol-ene click reaction in deep eutectic solvents for hydrophilic interaction chromatography. *J. Chromatogr. A* **1609**, 460446 (2020).
16. Yao A, et al. Flexible covalent organic network with ordered honeycomb nanoarchitecture for molecular separations. *ACS Nano* **17**, 22916-22927 (2023).
17. Li S, et al. Hydrophobic polyamide nanofilms provide rapid transport for crude oil separation. *Science* **377**, 1555-1561 (2022).
18. Jiang Z, et al. Aligned macrocycle pores in ultrathin films for accurate molecular sieving. *Nature* **609**, 58-64 (2022).
19. Li X, et al. Polycage membranes for precise molecular separation and catalysis. *Nat. Commun.* **14**, 3112 (2023).
20. Zheng D, et al. Polyamide composite membranes for enhanced organic solvent nanofiltration performance by metal ions assisted interfacial polymerization method. *AlChE J.* **69**, e17896 (2023).
21. Jin C-G, Zhang W-H, Tian N, Wu B, Yin M-J, An Q-F. Fabrication of coffee-ring nanostructured membranes for organic solvent nanofiltration. *Angew. Chem. Int. Ed.* **63**, e202405891 (2024).
22. Mi K, Xiong S, Lu Y, Wang Y. Precise fabrication of robust conjugated microporous polymer membranes via oxidative molecular layer deposition for efficient organic solvent nanofiltration. *Chem. Mater.* **36**, 7069-7078 (2024).